Chapter 5: Experimentation on SPNCL using water-based mono/hybrid nanofluids

In this chapter, an experimental investigation of the transient and steady-state performances of SPNCL using water and water-based mono/binary hybrid nanofluids has been carried out. This chapter consists of a detailed explanation of the preparation and characterization of nanoparticles and hybrid nanofluids, experimental setup and procedure, data analysis, and uncertainty analysis based on defined performance parameters. Finally, a detailed explanation of the effect of power input, coolant inlet temperature, and loop inclination (Counter-clockwise and Clockwise) on the performance parameter, i.e., mass flow rate, effectiveness of the heat exchanger, and total entropy generation rate, has been presented.

5.1 Preparation of and Characterization

5.1.1 Preparation of mono/hybrid nanofluids

The two-step method has been used to prepare mono/hybrid nanofluids in the present study, in which nanoparticles are purchased separately and then dispersed in the base fluid. The flow chart of the preparation of mono/hybrid nanofluids using the two-step method is illustrated in Fig. 5.1. Figure shows the preparation procedure of mono/hybrid nanofluids, nanoparticles, and equipment used for the preparation. Initially, the calculated amount of nanoparticles based on 0.1% volume concentration is measured in the electronic weighing machine (Model: ATX224, SHIMADZU, Japan) with an accuracy of ± 0.0001. Afterward, the measured quantity of nanoparticles is added to the base fluid (i.e., de-ionized water) and further stirred in a magnetic stirrer for 2 hours. Moreover, in order to get homogeneous dispersion and to avoid agglomeration, a Cetyltrimrthyl ammonium bromide (CTAB) surfactant has been added to the prepared mixture. Finally, the solution is sonicated by

ultrasonicator (Labman Scientific Instruments, India, 40kHz) for 6-8 hours for uniform dispersion of nanoparticles in the base fluid. The different types of nanoparticles, such as metal oxides (Al_2O_3, CuO), Carbon allotrope (MWCNT), and Carbide (SiC) are selected for the present study due to their different thermophysical properties and shape, as shown in Table 5.1. All the nanoparticles are purchased from Otto Chemika, Alfa Aesar, and the CTAB surfactant from SRL Company.

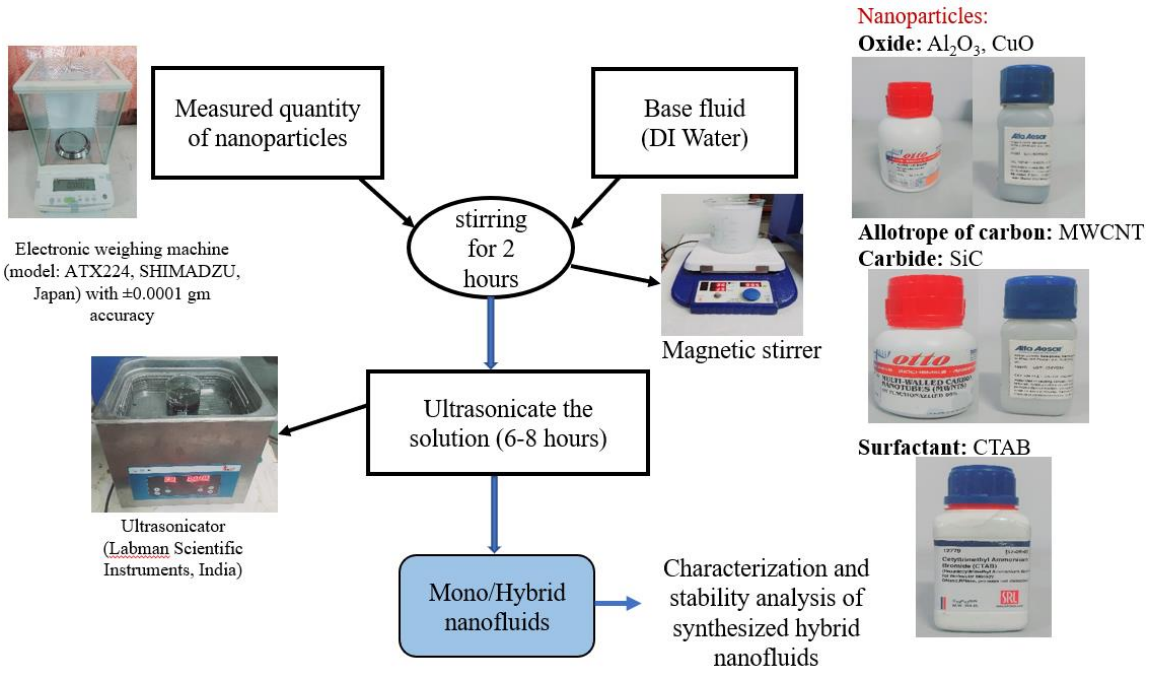

Fig. 5.1 Flow chart of preparation of mono/hybrid nanofluids, nanoparticles, and equipment used for the preparation of nanofluids

The volumetric capacity of the fabricated SPNCL is below 1 litre and hence the amount required for base fluid and nanoparticles to prepare 1 litre nanofluid has been calculated first.

At a given volume fraction of nanoparticles (ϕ) and total volume of mono nanofluid (V_{total}), the mass of nanoparticles and volume of base fluid are calculated by using the equation below;

$$m_{np} = \phi \rho_{np} V_{total} \qquad V_{bf} = (1-\phi) V_{total} \tag{5.1}$$

Similarly for given volume fractions of nanoparticles (ϕ_1, ϕ_2) and total volume of hybrid nanofluid (V_{total}), the mass of nanoparticles and volume of base fluid are estimated by,

$$m_{np1} = \phi_1 \rho_{np1} V_{total} \quad m_{np2} = \phi_2 \rho_{np2} V_{total} \quad V_{bf} = (1-\phi_1-\phi_2) V_{total} \tag{5.2}$$

In the present study, the nanoparticle mixing ratio ($\phi_1 : \phi_2$) is taken as (50:50).

Table 5.1 Particle size, shape, and thermophysical properties of nanoparticles used in the investigation [118]

Types of nanoparticles	**Average particle size, nm**	**Thermal conductivity (W/m.K)**	**Density (kg/m^3)**	**Specific heat (J/kg.K)**	**Shape**
Al_2O_3	< 50	36	3960	880	Spherical
CuO	< 50	33	6400	530	Spherical
SiC	50	350	3210	1340	Spherical
MWCNT	OD:20-30, Length:2 μm	3000	2600	740	Cylindrical

5.1.2 Characterization of nanoparticles

The morphology and distribution of the nanoparticle are obtained by using the scanning electron microscopy (HR-SEM), model EVO-Scanning Electron Microscope Ma15/18. Fig. 5.2 illustrates the SEM image of Al_2O_3 nanoparticle and Al_2O_3+MWCNT nanoparticles mixture. Fig. 5.2 (a) illustrates the SEM image of Al_2O_3 nanoparticle and discloses that the size of the Al_2O_3 nanoparticle is within 50 nm and spherical in shape as

predicted by ImageJ software. Whereas Fig.5.2 (b) illustrates the SEM image of Al_2O_3+MWCNT nanoparticles mixture and reveals that MWCNT has cylindrical in shape, having a length in the micrometer range, while Al_2O_3 has spherical in the shape of diameter < 50 nm.

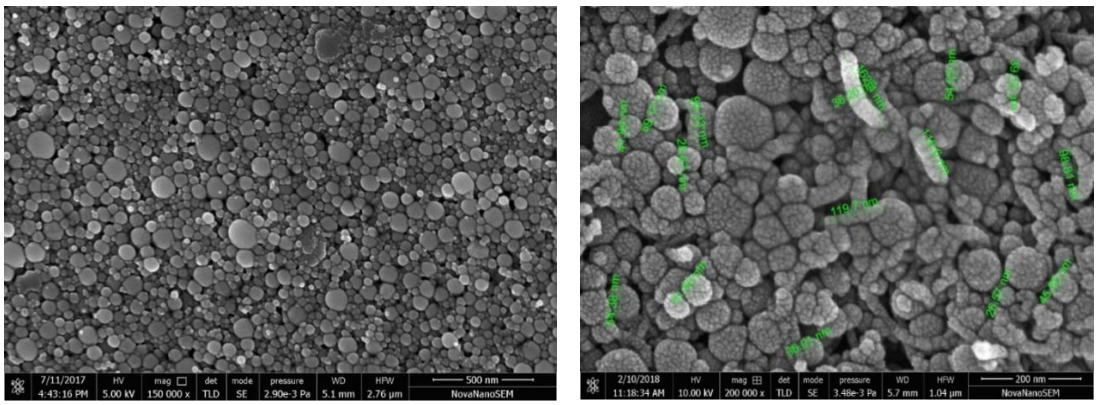

(a) Al_2O_3 (b) Al_2O_3+MWCNT

Fig. 5.2 SEM image (a) Al_2O_3 particle (b) Al_2O_3+CNT nanoparticles mixture

5.1.3 Stability of mono/hybrid nanofluids

In the present study, different water-based mono/hybrid nanofluids, i.e., Al_2O_3, Al_2O_3+CuO, Al_2O_3+SiC, and Al_2O_3+MWCNT of 0.1% total volume concentration of nanoparticle has been prepared. For binary hybrid nanofluids, an equal volume concentration (50:50) of each nanoparticle has been considered. The stability of mono/hybrid nanofluids has been observed using the photographic method. In this method, all the prepared mono/hybrid nanofluids are kept for visual observation. The photographs of mono/hybrid nanofluids are presented with time (maximum 20 days) to observe the stability of prepared hybrid nanofluids, from which the sedimentation of dispersed nanoparticles can be observed from the naked eyes shown in Fig. 5.3**.** The figure reveals that Al_2O_3+Water and Al_2O_3+CuO+Water shows nearly complete sedimentation in 10 days and 20 days respectively. Whereas, Al_2O_3+SiC+water shows partial sedimentation and

Al_2O_3+MWCNT+water shows no sedimentation after 20 days. Which is adequate time to conduct the present experimental investigation, since the time required to perform a set of experiments with one type of nanofluid is about 2 days.

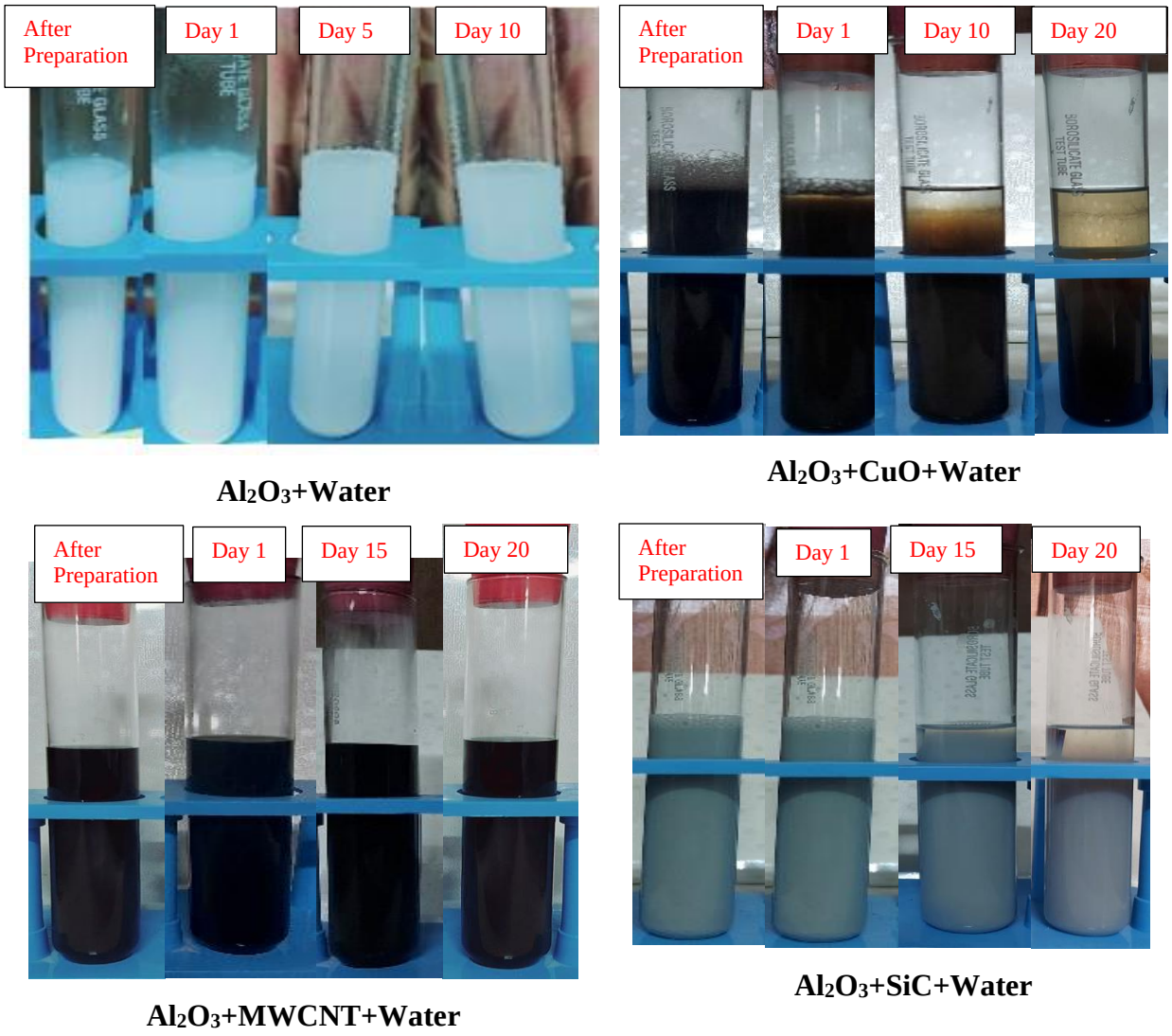

Fig. 5.3 Photographs of prepared nano/hybrid nanofluids with time

5.1.4 Calculation of thermophysical properties of nanofluids

All the thermophysical properties of the mono/hybrid nanofluids have been calculated by using models and correlations, as discussed in chapter 3. The temperature-dependent thermophysical properties of the base fluid (water) are taken from the EES library [111].

5.2 Experimentation methodology

5.2.1 Experimental setup and instrumentation

The schematic layout of the experimental facility and photographic view of the experimental test rig are presented in Fig. 5.4(a) and Fig. 5.4(b), respectively. The system consists of three main units; primary fluid circulation loop, secondary fluid circulation loop, and measuring unit. The primary fluid circulation loop consists of a rectangular-shaped smooth circular cross-section copper pipe, heating and cooling sections, and an electromagnetic flow meter. Rectangular shaped loop has a total loop length of 4m, with 1.2 m in height and 0.8 m in width of the loop, and the inner diameter of the copper tube is 13.6 mm and 1 mm in thickness. Heating section consists of an electrical heating wire made of nicromel on the outside of the copper tube of heating length 0.5 m mounted 0.1 m above in the left vertical arm from the bottom of the rectangular loop. The cooling section consists of a coaxial cylindrical heat exchanger of a cooling length of 0.6 m mounted on the top horizontal arm. An electromagnetic flow meter has been mounted on the right vertical arm to measure the volume flow rate of the primary fluid. The secondary fluid circulation loop consists of piping, a temperature controller bath, magnetic pump for the continuous circulation of the secondary fluid through the cooling section. The measuring unit consists of a Variac, Wattmeter, and Data acquisition system (NI 9214-DAQ). In order to prevent convective and radiative heat losses to the ambient, the entire loop is insulated with 25 mm thick ceramic padding. The loop is operated under atmospheric condition; therefore, an expansion tank is mounted at the top left horizontal arm of the loop to release the excess pressure. Also it helps to make sure that the rectangular loop is completely filled. To investigate the effect of loop inclination locking system is attached, which enables the loop to inclined on both Counter-clockwise and Clockwise, protractor is used to fix the loop at a specific angle. To measure the temperature of the primary fluid, Heater wall temperature,

secondary fluid inlet and outlet, Insulation surface temperature, and ambient temperature, K-type thermocouples are placed at different locations shown in Table 5.2. These thermocouples are connected to a computer-integrated data acquisition system (NI-DAQ) to record the temperature data at regular intervals. To measure the secondary fluid flow rate, a rotameter is connected between the thermostatic bath and heat exchanger inlet. The geometrical and material specifications of the loop have been provided in Table 5.3. The list of instruments and their specification used to measure the different parameters are provided in Table 5.4.

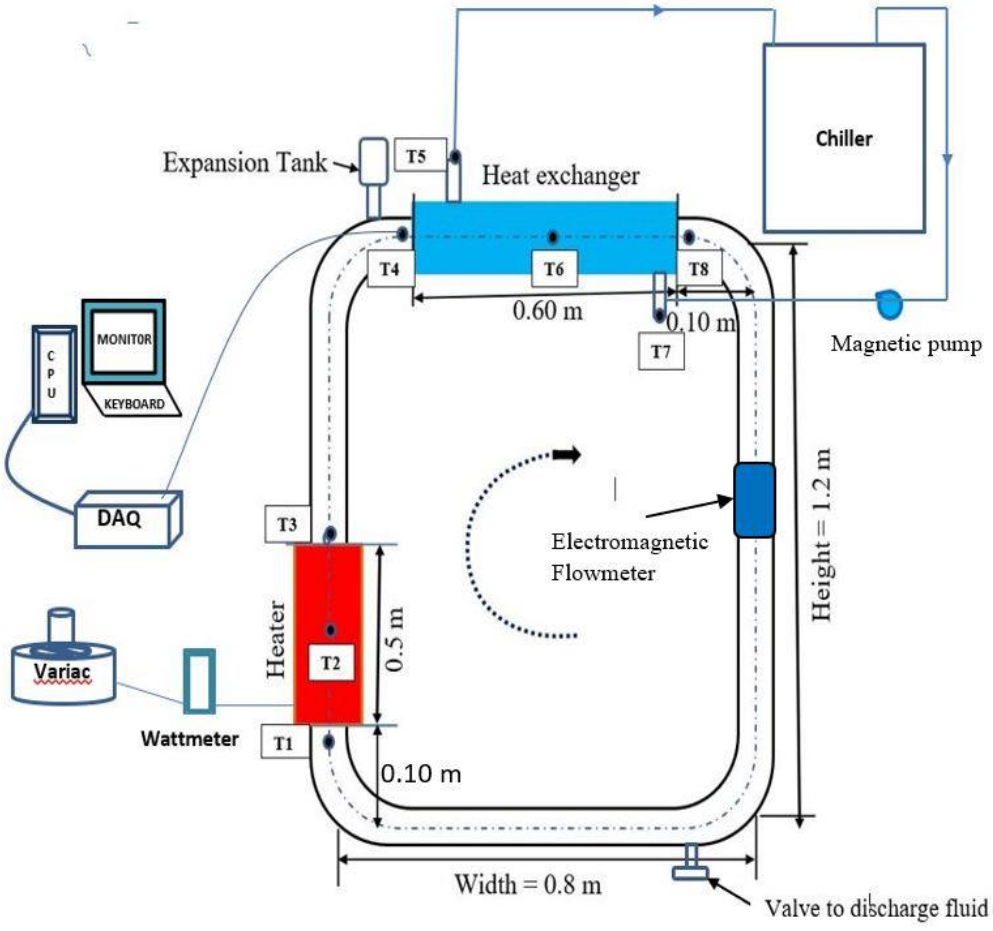

(a)

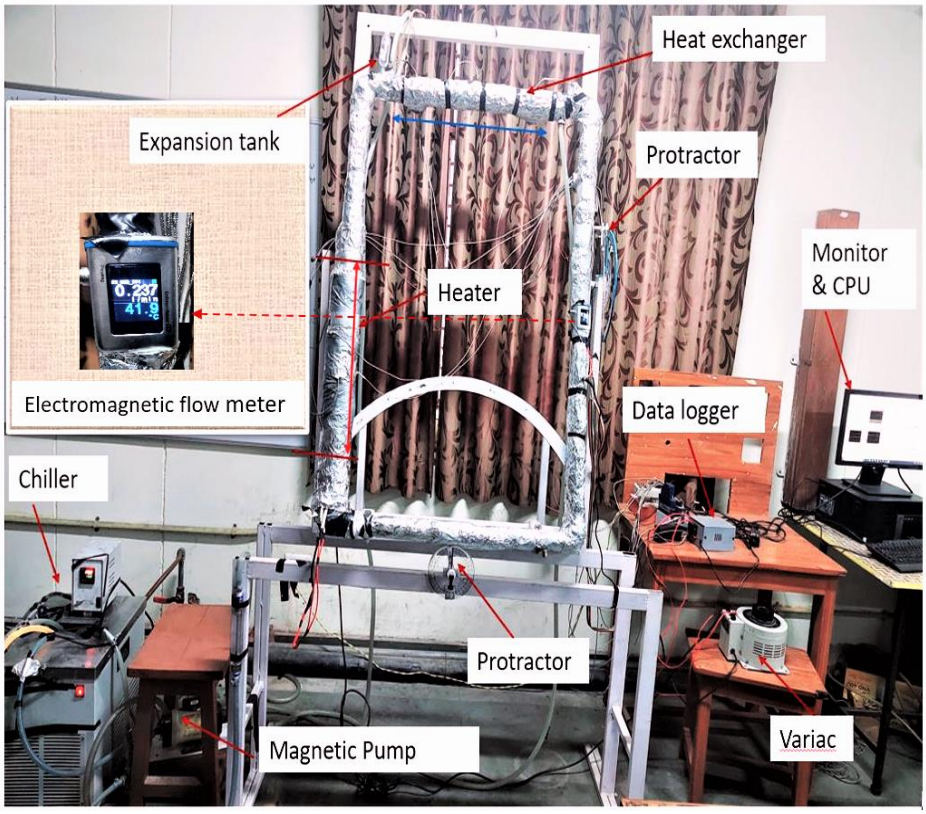

(b)

Fig. 5.4 (a) Schematic layout out Experimental facility, (b) Photographic view of Experimental facility.

Table 5.2 Position of the thermocouples

Thermocouple number	**Position**
T_1	Heater inlet
T_2	Heat wall surface
T_3	Heater outlet
T_4	Heat exchanger inlet
T_5	Coolant inlet
T_6	Heat exchanger surface
T_7	Coolant outlet
T_8	Heat exchanger inlet

T_9	Heating section insulation surface
T_{10}	Ambient Temperature

Table 5.3 Geometric parameters and materials used in the experimentation.

Geometric dimensions and materials	**Values**
Loop diameter (internal)	13.6 mm
Thickness	1 mm
Loop Height	1.2 m
Loop width	0.8 m
Heating length	0.50 m
Cooling length	0.60 m
Tube wall material	Copper
Insulation thickness	25 mm
Expansion tank	Borosilicate glass
Insulation material	Ceramic pads

.

Table 5.4 Instruments and their specification used to measure the different parameters

Parameters	**Instruments**	**Measurement range**	**Accuracy**
Temperature	K type thermocouple	20 to 300 ºC	$\pm$0.33 ºC
Flow rate	Electromagnetic flowmeter	0 to 20 LPM	$\pm$0.20%

Wattmeter	Specification: 250 V, 50 Hz, Max. 10 A	Less than 2.2 KW	$\pm$0.25%

5.2.2 Experimental procedure

The experiments are performed for different water and water-based working fluid such as DI water, Al_2O_3+Water, Al_2O_3+CuO+Water, Al_2O_3+SiC+Water, Al_2O_3+MWCNT+Water. After completion of each set of experiments using nanofluids, the entire rectangular loop is cleaned by using DI water to conduct the experiment for the next working fluid. In this investigation, the effect of different power inputs, Coolant (Secondary fluid) inlet temperature, and loop inclination (Counter-clockwise and Clockwise) have been investigated. The following steps have been carried out to perform the experiment. Firstly, the loop was filled with the working fluid, and air bubbles are drained out completely. The secondary fluid (coolant) i.e., water at a specified temperature and flow rate is circulated through the heat exchanger, and sufficient time is provided to achieve uniform temperature in the loop. The high mass flow rate of coolant is kept to maintain the negligible coolant outlet and inlet temperature difference to impose the constant sink temperature condition. After ensuring the uniform temperature in the loop, the heater is set at a specified power input and then the heater and DAQ system are switched on simultaneously. All the temperature data measured by K-type thermocouple and flow rate data by electromagnetic flowmeter are recorded by NI DAQ over a period of 4000 s (Steady state is achieved) at 2 sec of time interval. The steady-state is ensured by recording the practically unchanged (relatively less than 2%) values for the recorded working fluid temperature. Each set of experiments is performed three times to ensure repeatability. The same procedure is repeated for each set of experiments.

5.2.3 Data analysis and performance parameter

Three important performance parameters, viz. buoyancy force-induced mass flow rate, effectiveness of cooler, and the total entropy generation rate, are used for comparing the different working fluids. This provides the energy-exergy performance of the loop. These performance parameters are calculated by;

b. ***Buoyancy force-induced mass flow rate of the working fluid inside the loop***:

$$\dot{m} = (\dot{V}\rho) / (1000 \times 60) \tag{5.3}$$

Where, $\dot{V}$ is the volume flow rate in LPM measured by the electromagnetic flow meter and ρ is the density of the primary fluid.

c. ***Effectiveness of the cooler:*** It is defined by the ratio of actual heat transfer to the maximum possible heat transfer through the cooler. It predicts the heat transfer capability of the system as given by [52],

$$\varepsilon = \frac{T_{C,in} - T_{C,out}}{T_{C,in} - T_{S,in}} \tag{5.4}$$

Where, $T_{C,in}$ and $T_{C,out}$ are the inlet and outlet temperature of the primary fluid in the heat exchanger, and $T_{S,in}$ is the secondary fluid inlet temperature.

d. ***The total entropy generation rate of the loop***: It has been derived by using the entropy balance principle. It predicts the exergetic performance of the system. The entropy generation rate for different heating, cooling, hot and cold leg sections is given by equation (5.5, 5.6, and 5.7) respectively,

$$S_{gen,H} = \dot{m}\left[c_p \ln\left(\frac{T_{H,out}}{T_{H,in}}\right) + \frac{fL_H \dot{m}^2}{2d\rho_{H,avg}^2 A^2 T_{H,avg}} - \frac{c_p\left(T_{H,out} - T_{H,in}\right)}{T_{wall,H}} \right] \tag{5.5}$$

Entropy generation rate in the cooling section is derived by neglecting the irreversibility due to pressure drop of the coolant fluid.

$$S_{gen,C} = \dot{m}\left[c_p \ln\left(\frac{T_{C,out}}{T_{C,in}}\right) + \frac{fL_C\dot{m}^2}{2d\rho_{C,avg}^2 A^2 T_{C,avg}} \right] + m_S c_{p,S} \ln\left(\frac{T_{S,out}}{T_{S,in}}\right) \quad (5.6)$$

$$S_{gen,leg} = \frac{f\dot{m}^3}{2dA^2}\left[\frac{L_h}{\rho_{h,avg}^2 T_{h,avg}} + \frac{L_c}{\rho_{c,avg}^2 T_{c,avg}} \right] \quad (5.7)$$

Thus, the total entropy generation rate in the SPNCL is provided by,

$$S_{gen,t} = S_{gen,H} + S_{gen,C} + S_{gen,leg} \quad (5.8)$$

Where, $T_{H,in}$, $T_{H,out}$, $T_{S,in}$, $T_{S,out}$ are the inlet and outlet temperature of the primary fluid in the heater and Secondary fluid in the heat exchanger.

$T_{H,avg}$, $T_{C,avg}$ are the mean inlet and outlet temperature of the primary fluid in the heater, cooler, hot, and cold leg, respectively.

5.2.4 Uncertainty analysis

The uncertainty estimation of the dependent parameters such as mass flow rate, effectiveness of the heat exchanger, and total entropy generation rate are calculated using equation (5.9) given by (Kline and McClintock, 1953) [119].

$$U_Z = \left[\left(\frac{\partial Z}{\partial X_1} i_1\right)^2 + \left(\frac{\partial Z}{\partial X_2} i_2\right)^2 + \ldots\ldots\ldots + \left(\frac{\partial Z}{\partial X_n} i_n\right)^2 \right]^{\frac{1}{2}} \quad (5.9)$$

Where, Z is a function of the independent variables X_1, X_2, X_3,…,X_n and i_1, i_2, i_3,….,i_n are the uncertainties of the independent variables. The maximum uncertainties of the calculated parameters are listed in Table 5.5.

Table 5.5 Maximum uncertainties of the calculated parameters

Parameters	**Uncertainty value (%)**
Mass flow rate	±0.8

Effectiveness, ε	±2.6
Total entropy generation rate, $S_{gen,t}$ (W/K)	±2.2

5.3 Results and discussion

In the present experimental investigation, the effect of different water and water-based mono/hybrid nanofluids, power input, coolant inlet temperature, and loop inclination on the steady and transient performance of VHHC SPNCL has been studied. The operating condition parameters are provided in the given Table 5.6.

Table 5.6 Operating parameters of VHHC SPNCL.

Input Parameters	Values/Range	Mean value
Power input	200, 400, 600, 800 W	400 W
Coolant inlet temperature	295, 305, 315 K	295K
Loop inclination	0^o, 30^o, 60^o	0^o
Coolant flow rate	5 LPM	-
Pressure inside loop	101.325 kPa	-
Type of nanoparticles	Al_2O_3, CuO, SiC, CNT	-
Working fluids	Water, Al_2O_3+Water, Al_2O_3+CuO+Water, Al_2O_3+SiC+Water, Al_2O_3+CNT+Water	-
Nanoparticle volume concentration	$\phi = 0.1\%$	-

5.3.1 Repeatability test

The repeatability of the reported experiments is ensured through a direct comparison of the measured mass flow rate for an input power of 400 W using water as the working fluid. The fig. 5.5 shows the measured transient mass flow rate in three different experiments for a particular loop arrangement, input power of 400 W, and coolant inlet temperature of 295 K (see Fig. 5.5). The analyses of transient data revealed a deviation of less than 2% between the different experiments. Thus, the quality of reported data is ascertained.

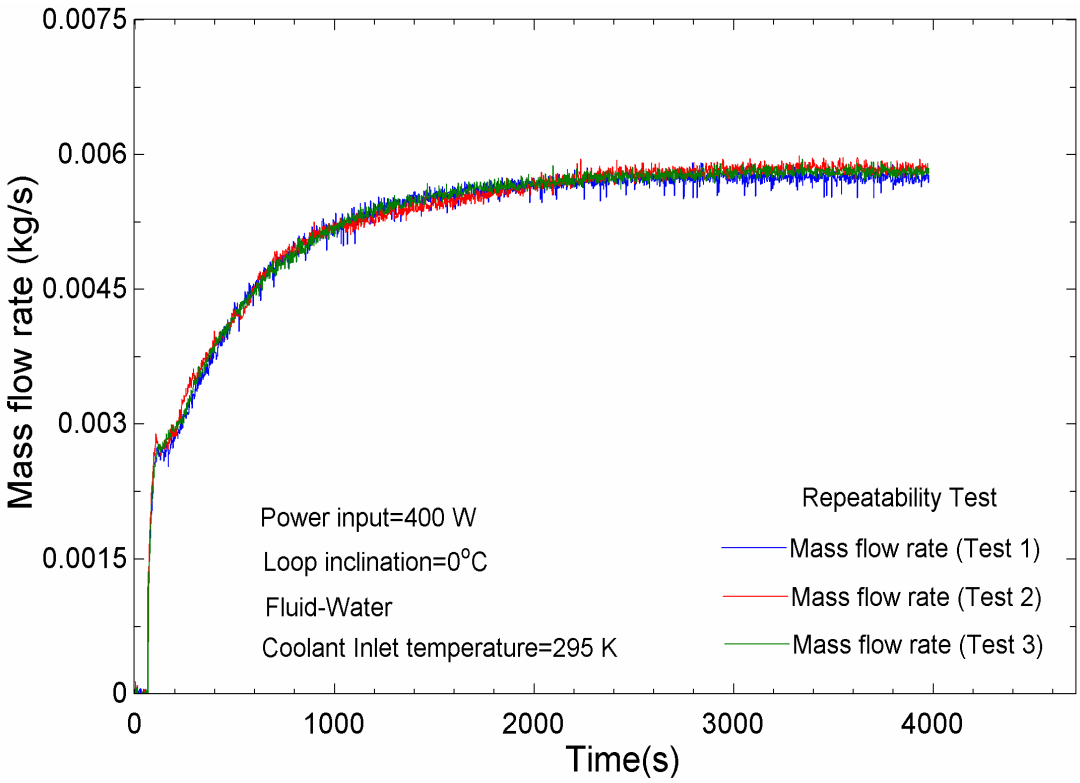

Fig. 5.5 The measured water mass flow rate for three different experiments under an identical operating condition to ensure repeatability.

5.3.2 Comparison of the experimental and numerical results

In this section, the experimental transient mass flow rate is compared with the numerical result at different power inputs for water, as shown in Fig.5.6. The details of the numerical code have been discussed in Chapter 4 (Case vi). From the figure, it can be seen that the

experimental and numerical results are well in the steady-state region (after 1200 s); however, a little deviation can be observed in the transient region in the flow initiation and the maximum deviation is observed for the mass flow rate.

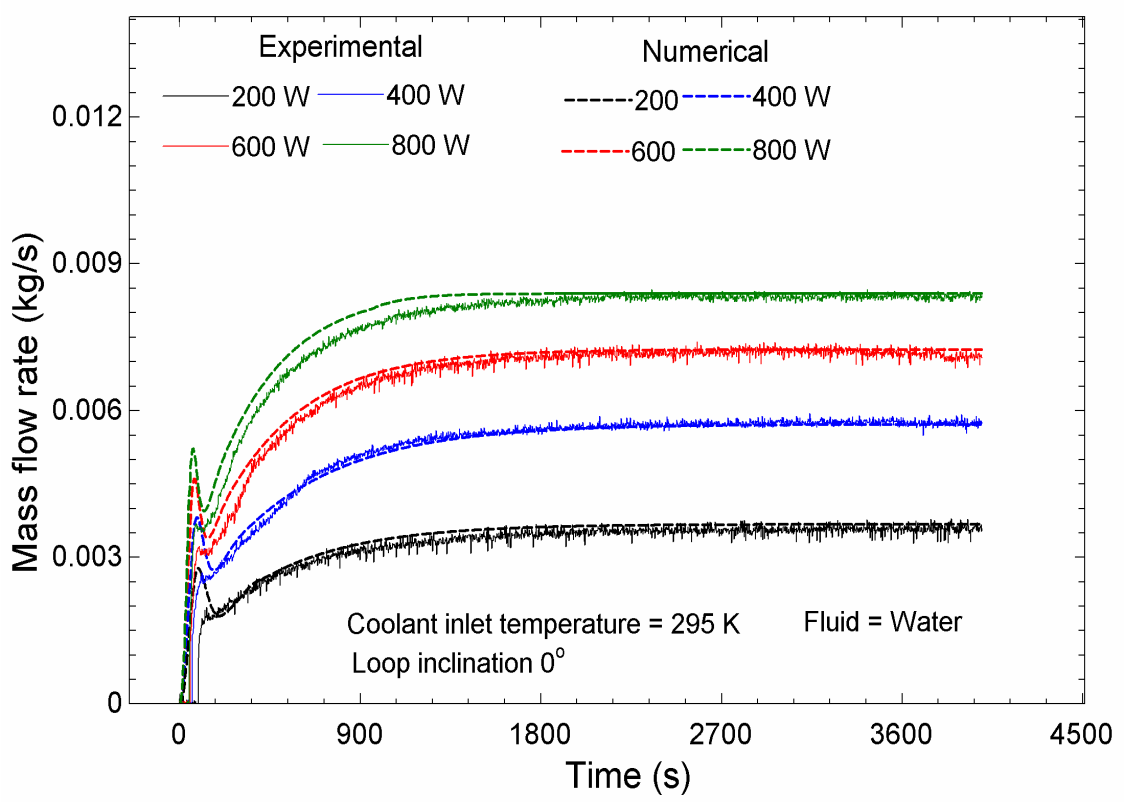

Fig. 5.6 Comparison of experimental transient mass flow rate with the numerical result for different power inputs

5.3.3 Transient behavior of SPNCL for various hybrid nanofluids

Figure 5.7 show the transient mass flow rate for various water and water-based mono/hybrid nanofluids at 400 W. All the fluids show similar trend, i.e., flow initiation, attaining a maximum peak, decrease in the mass flow rate, then increase the mass flow rate, and finally achieving steady state. The reason for this trend is due to the interplay between buoyancy force and frictional force. The domination of buoyancy force accelerates the flow, while the domination of frictional force deaccelerates the flow. When these two forces

balance each other, the mass flow rate becomes constant and attains a steady state. The flow initiation time is different for different working fluids; all the hybrid nanofluids take a longer flow initiation time, 64 s, 67 s, and 74 s for Al_2O_3+water, Al_2O_3+CuO+water, Al_2O_3+MWCNT, respectively, except Al_2O_3+SiC+water (58 s) compared to water (60 s) depicted in zoomed view in Fig 5.7. Moreover, an increase in mass flow rate is observed for Al_2O_3+water (2.20%) and Al_2O_3+SiC+water (1.30%), and a reduction in mass flow rate is observed for Al_2O_3+CuO+water (1.25%) and Al_2O_3+MWCNT+water (6%) compared to water at 400 W power input. This is because buoyancy force increases with density, the temperature difference between hot and cold legs (decreasing specific heat), and the thermal expansion coefficient for hybrid nanofluids. On the other hand, the friction loss increases with viscosity and density. Adding nanoparticles to the water, both viscosity, and density increase so the friction force increases. Therefore, the increase or reduction in mass flow rate of hybrid nanofluids compared to water depends on the domination of net change in buoyancy force and friction force. The dominance of the buoyancy force enhances the mass flow rate, while the dominance of the viscous force reduces the mass flow rate. Fig. 5.7 also demonstrates the mass flow rate is higher for spherical shaped based hybrid nanofluids (Al_2O_3+water, Al_2O_3+SiC+water, and Al_2O_3+CuO+water) compared to cylindrical-shaped hybrid nanofluid Al_2O_3+MWCNT+water. These clearly show that the shape and properties of nanoparticle influences the mass flow rate. The lower mass flow rate of hybrid nanofluid having a cylindrical shape (Al_2O_3+CNT+water) is due to higher viscosity. A high viscosity may be due to the large surface area to volume ratio of the nanoparticles. More surface area increases the friction among nanoparticle and fluid particles, increasing the viscosity and, hence, increasing frictional force; as a result, a decrease in mass flow rate. Fig. 5.8 shows the temporal heater temperature difference for different working fluids at 400 W. The heater temperature difference is higher for

Al_2O_3+CuO+Water and lowest for Al_2O_3+SiC+water hybrid nanofluids, and this is because the heater temperature difference depends on the product of mass flow rate and specific heat of the working fluids at a given power input under steady-state. The Al_2O_3+CuO+Water has a lower mass flow rate and specific heat capacity, while Al_2O_3+SiC+water has a higher mass flow rate and specific heat.

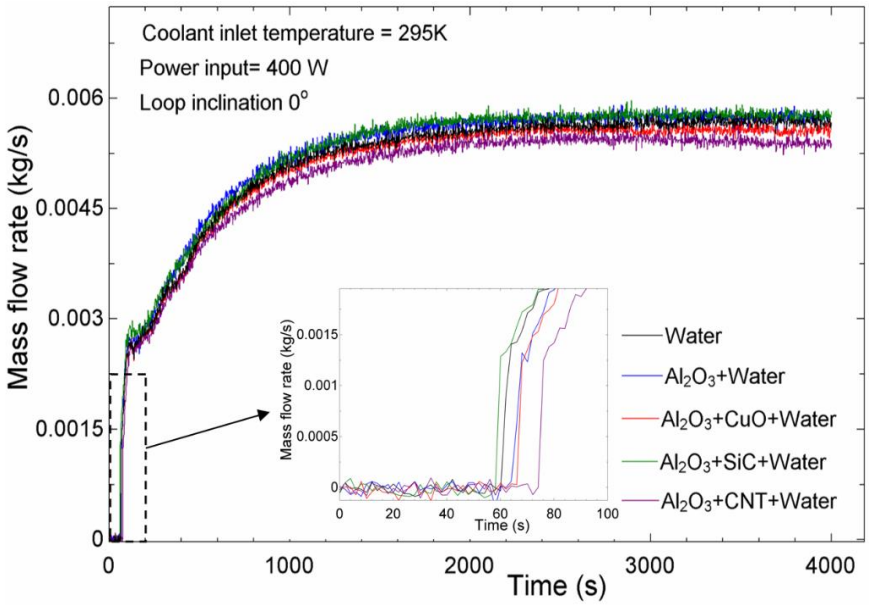

Fig. 5.7 Experimental transient mass flow rate for different mono/hybrid nanofluids.

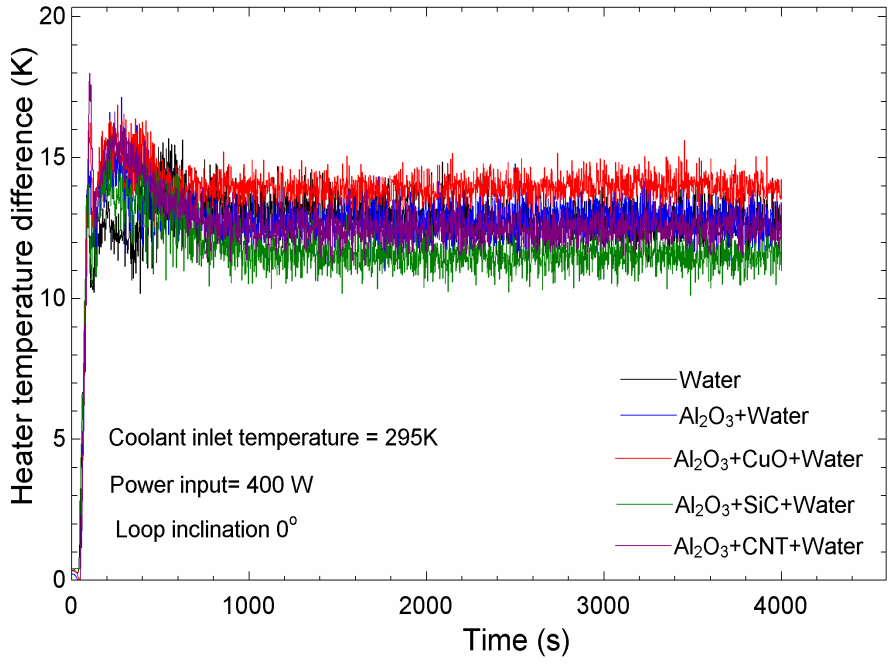

Fig. 5.8 Experimental transient heater temperature difference for different Fluids.

5.3.4 Influence of input power on steady-state performance parameter

The steady-state mass flow rates for water-based mono/hybrid nanofluids and water at different input powers are illustrated in Fig. 5.9. This shows that the mass flow rate increases with the input power for all the working fluids. This may be attributed to a higher temperature difference between cold and hot legs, which increases the buoyant force relative to the pressure drop. It may be inferred that the spherical-spherical nanoparticle-based mono/hybrid nanofluid has a higher mass flow rate, whereas for Al_2O_3+MWCNT+Water has a lower mass flow rate. The maximum increments in mass flow rate observed at the highest power input 800 W for Al_2O_3+water (5.5%) followed by Al_2O_3+SiC+water (4.3%) and Al_2O_3+CuO+water (1.9%) compared to water. Whereas 2% reduction in mass flow rate is observed for Al_2O_3+MWCNT+water. The possible reason is that at lower input power, the flow is under laminar regimes, so the increase in frictional force for hybrid-nanofluids due to nanoparticle suspension is more dominant than the buoyancy force. As the input power increases, the flow regime changes from laminar to turbulent, and therefore, the relative effect of frictional force decreases because of lower dominance of viscosity, and buoyant force starts dominating because of the suspended nanoparticles. This observation infers that the addition of nanoparticles at a high input power is more beneficial compared to low input power.

The steady-state effectiveness of the heat exchanger for water and water-based mono/hybrid-nanofluids at different input power has been shown in Fig. 5.10. The Figure illustrates the effectiveness decreases with the input power for all the working fluids. The mono/hybrid nanofluids show higher effectiveness compared to the water. The Al_2O_3+CNT+Water shows higher effectiveness compared to water as well as other hybrid nanofluids. This is because at a given power input the Al_2O_3+CNT+Water has a lower mass flow rate, which increases the temperature difference between the inlet and outlet of the

heat exchanger, i.e., increasing the numerator term of equation (5.4), also due to higher thermal conductivity of the nanofluid, the outlet temperature of the heat exchanger decreases which decreases the denominator term; as a result, effectiveness increases.

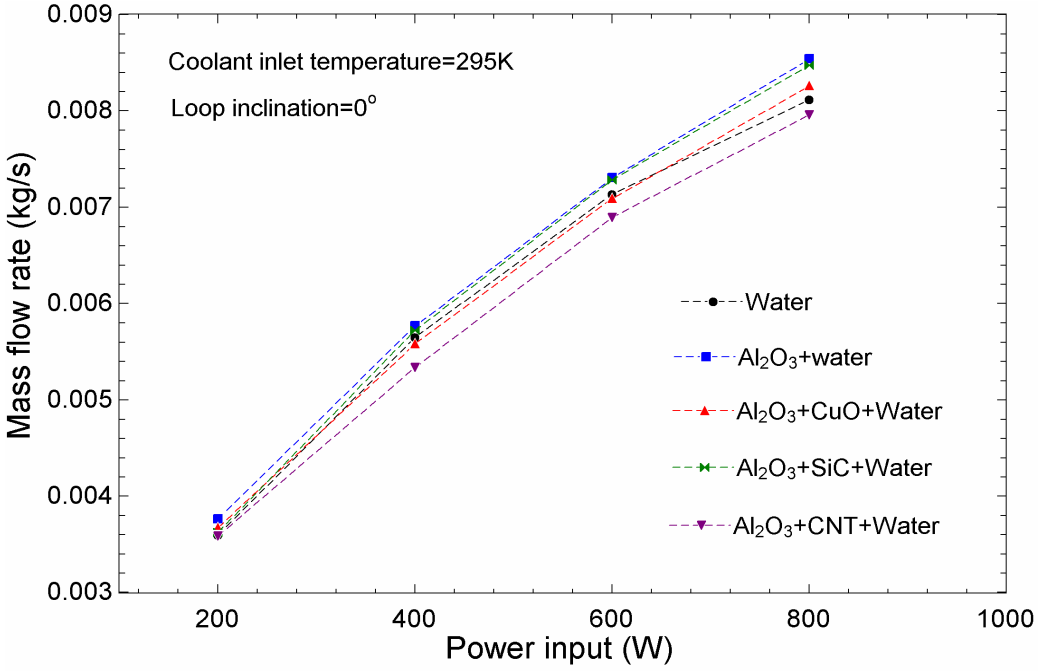

Fig. 5.9 Steady-state mass flow rate for different mono/hybrid nanofluids at power input.

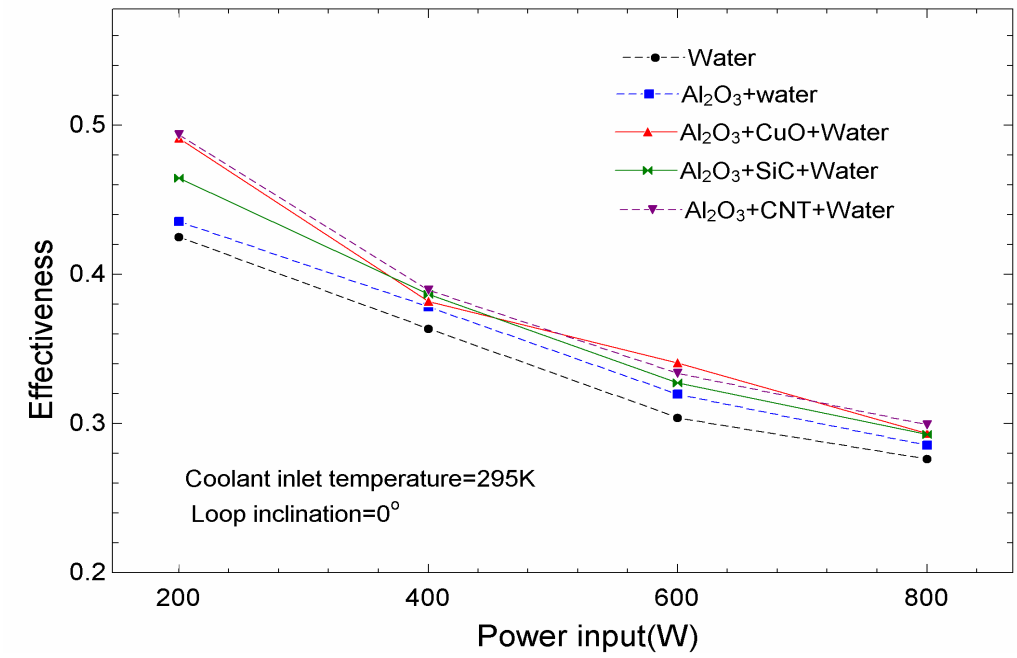

Fig. 5.10 Steady state effectiveness for different water-based mono/hybrid nanofluid at different power input

The maximum increment in effectiveness is for Al_2O_3+CNT+Water (16%) followed by Al_2O_3+CuO+Water (15%), Al_2O_3+SiC+Water (9.5%), and Al_2O_3+Water (2.5%) at 200 W power input compared to water.

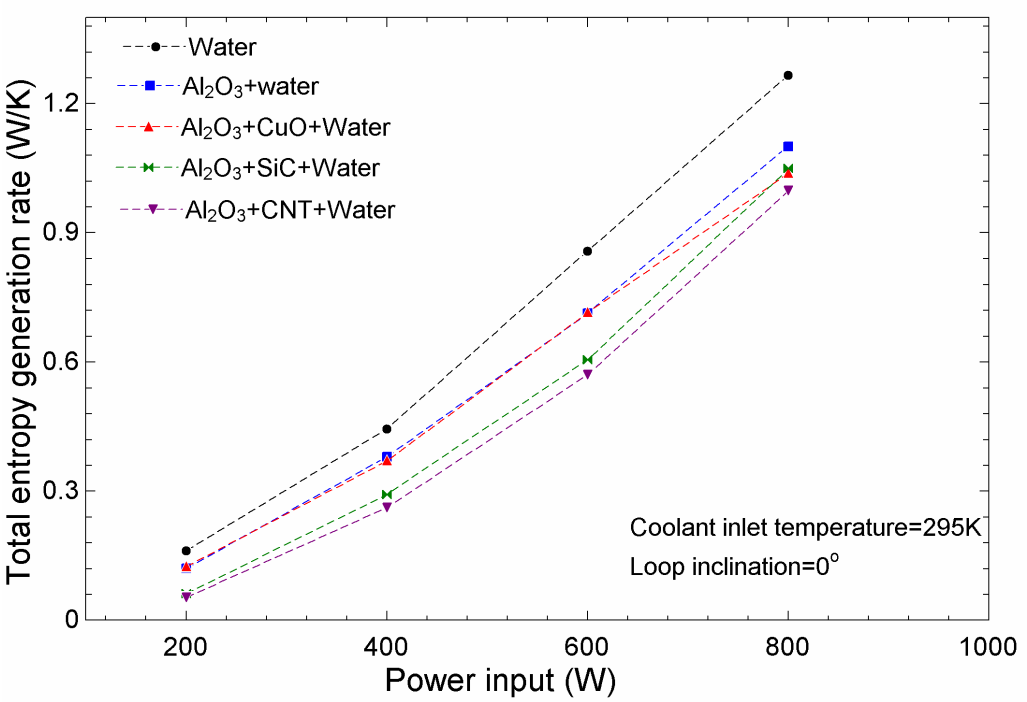

Fig. 5.11 Steady state total entropy generation rate for different mono/hybrid nanofluids at different power input

Fig. 5.11 demonstrates the variation of total entropy generation in the loop with respect to heater power input for different mono/hybrid nanofluids and water. It depicts that the entropy generation increases with increasing power input. The possible reason is that the entropy generation depends on the irreversibility due to heat transfer and pressure drop. As the power input increases, the heat transfer and pressure drop increase; hence, the entropy generation increases. At a given power, it can be observed that the entropy generation for water is found to be higher than all mono/hybrid nanofluids. Al_2O_3+CNT+water shows a minimum total entropy generation rate compared to water and other binary hybrid nanofluids. The maximum reduction in total entropy generation rate is for

Al_2O_3+CNT+Water (21%) followed by Al_2O_3+CuO+Water (18%), Al_2O_3+SiC+Water (17%), and Al_2O_3+Water (13%) at 800 W power input compared to water.

5.3.5 Effect of coolant inlet temperature on the performance parameters

Fig.5.12 demonstrates the effect of coolant inlet temperature on the temporal mass flow rate at a 400 W power input for water. It is observed that the mass flow rate increases with increasing coolant inlet temperature. This is because at higher coolant inlet temperature, the average temperature of the loop increases, which decreases the viscosity of the working fluid and hence reduces the frictional force. Moreover, the buoyancy force also increases because the change in the density difference is more at higher temperatures for the same temperature difference. The flow initiation of the working fluid is earlier at higher coolant inlet temperature (see the zoom view in Fig. 5.12).

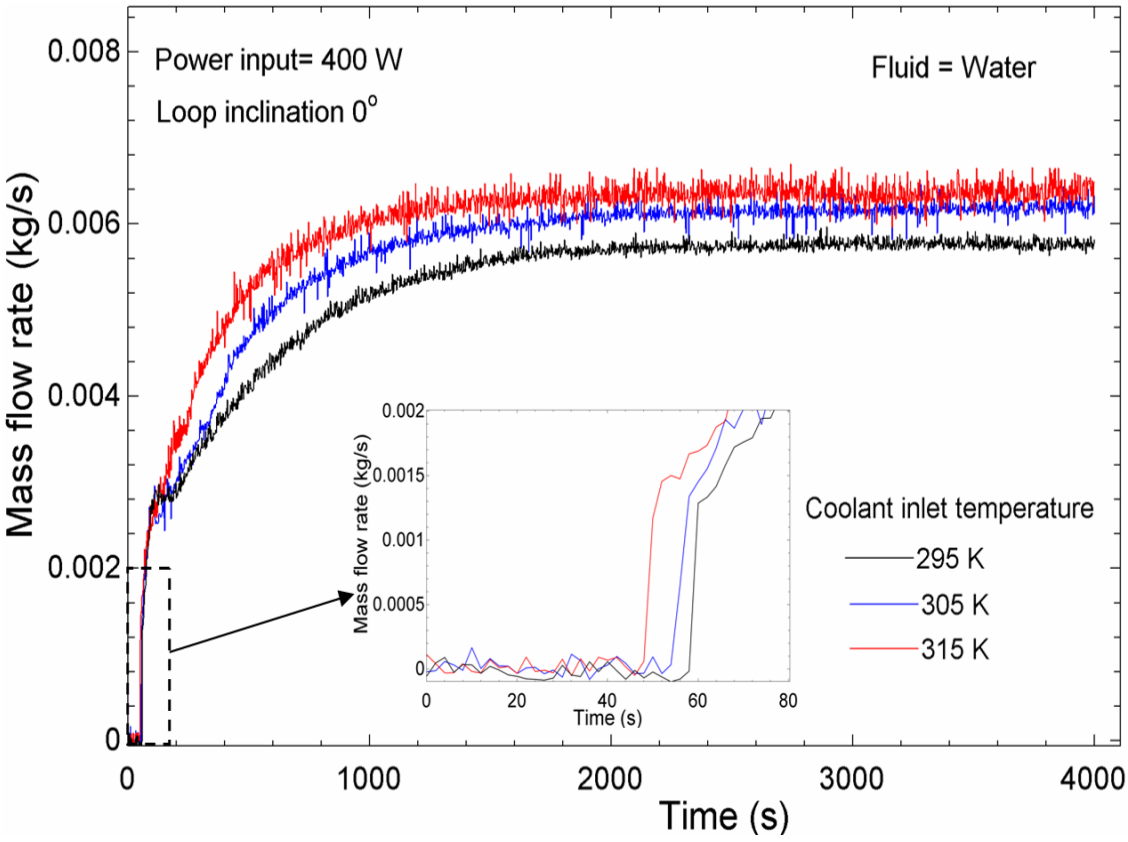

Fig. 5.12 Experimental transient mass flow rate at different coolant inlet temperatures

Fig. 5.13 demonstrates the effect of coolant inlet temperature on the steady-state mass flow rate for different working fluids. It can be seen that the mass flow rate of all the working fluids increases with the coolant inlet temperature. But the rate of increment of mass flow rate reduces with increasing coolant inlet temperature. The change in mass flow rate is 6.5% and 1.9% when coolant inlet temperature changes from 295K to 305K and 305K to 315K, respectively.

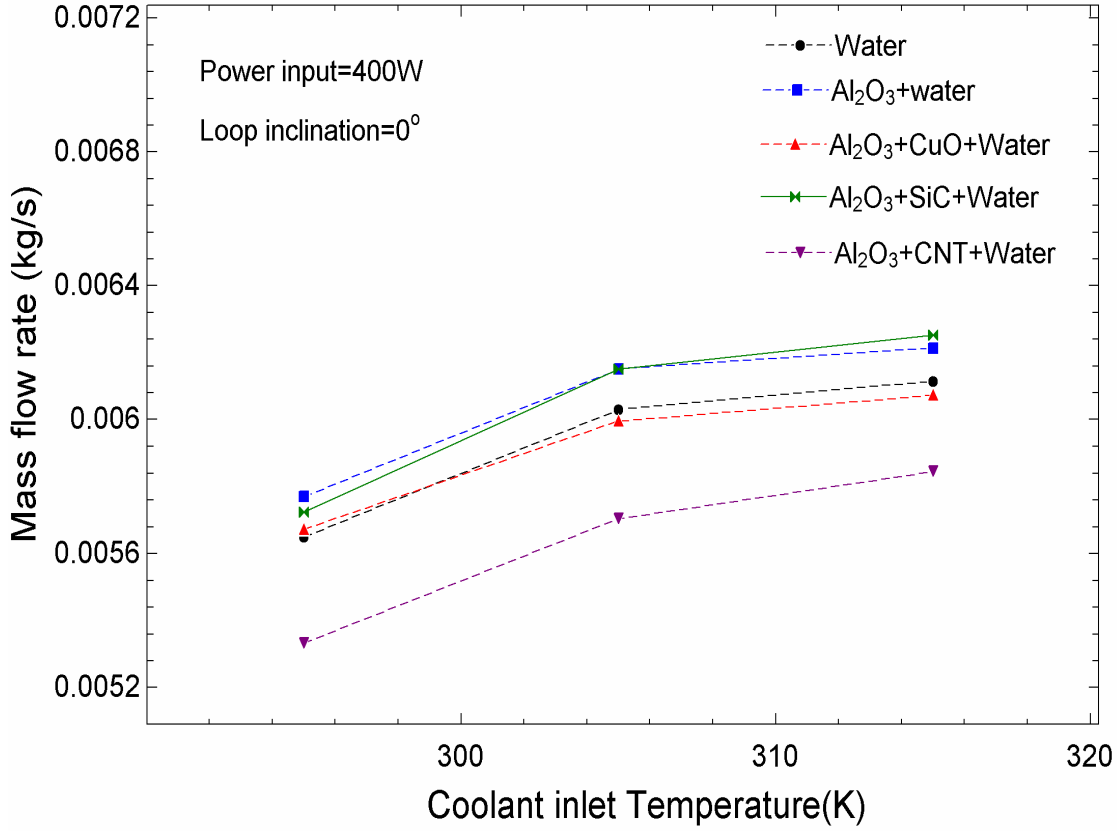

Fig. 5.13 Steady state experimental mass flow rate for different water-based mono/hybrid nanofluids at different coolant inlet temperatures

Fig.5.14 illustrates that the effectiveness of the cooler decreases with increasing the coolant inlet temperature. This is because as coolant inlet temperature increases, both numerator and denominator in the effectiveness equation (5.4) decrease but the decrement in the numerator term is higher than the denominator; hence the effectiveness decreases. The change in effectiveness is more significant at a lower coolant inlet temperature. This is

because the change in effectiveness is about 17% and 1.9% when coolant inlet temperature changes from 295K to 305K and 305K to 315K, respectively.

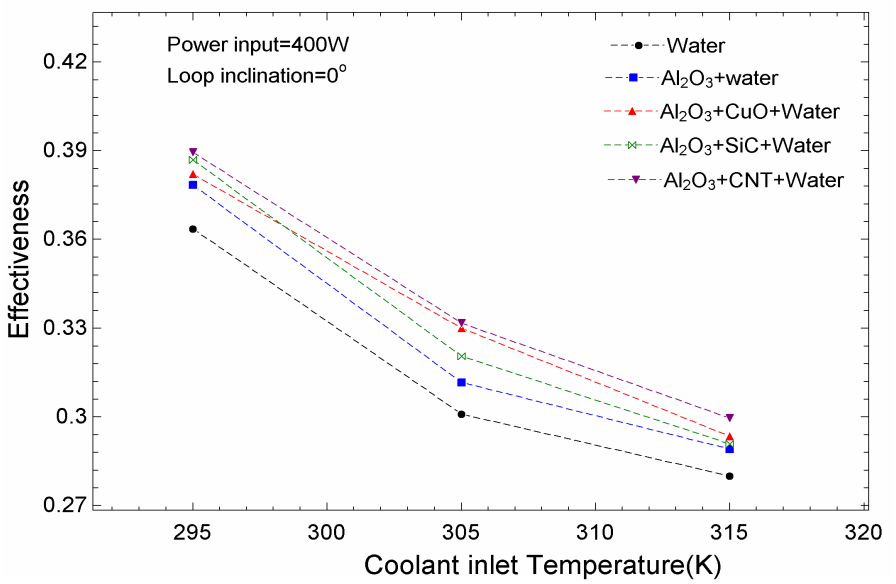

Fig. 5.14 Steady state experimental effectiveness for different water-based mono/hybrid nanofluids at different coolant inlet temperatures

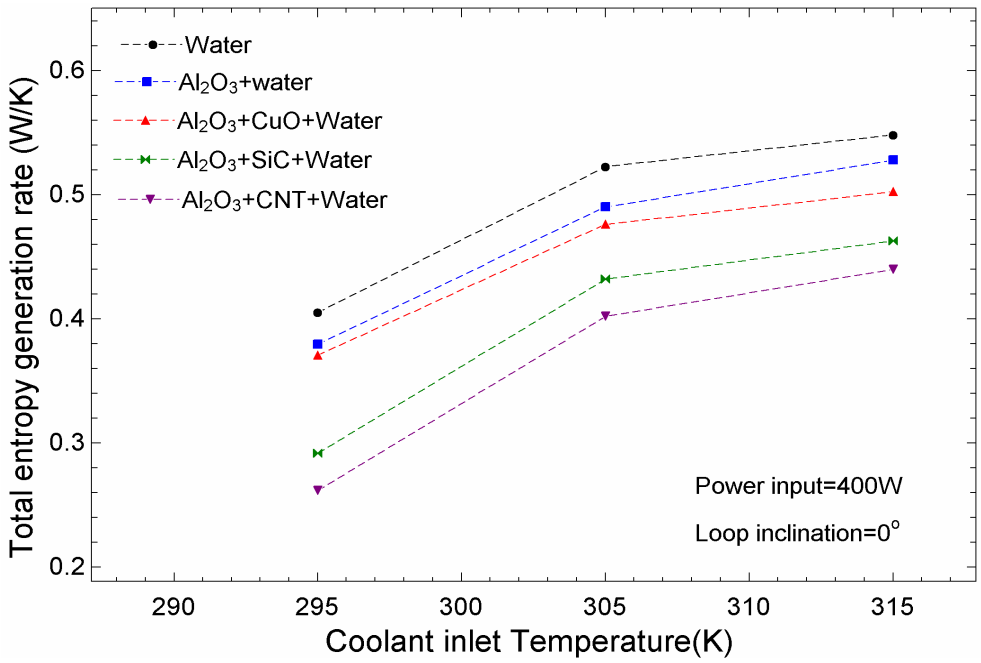

Fig. 5.15 Steady state experimental total entropy generation rate for different water-based mono/hybrid nanofluids at different coolant inlet temperatures.

Fig.5.15 demonstrates that the entropy generation rate is more at a higher coolant inlet temperature for all the working fluids. The possible reason is that at higher coolant temperature, the mass flow rate and the average temperature of the loop increase, which increases the irreversibility due to pressure drop and heat transfer, respectively, hence increasing the total entropy generation rate.

5.3.6 Effect of loop inclination on the performance parameter

In this section, the effect of the inclination of the loop on both the Counter-clockwise and Clockwise has been investigated, as shown in Fig. 5.16 (a) and (b), respectively. The Counter-clockwise inclination of the loop is considered as a "-ve" sign, whereas the Clockwise inclination is considered as a "+ve" sign to represent in the graph.

(a) (b)

Fig. 5.16 a) Counter clockwise inclination of the loop, (b) Clock wise inclination of the loop from vertical

Figure 5.17 shows the temporal variation of mass flow rate at a different angle of inclination for water at 400 W power input. It can be observed that the mass flow rate is maximum

flow vertical (0^0) loop and lowest for Clockwise (60^0) inclination. Although the loop is inclined at the same angle for both right and Counter-clockwises, the right-side inclination has a lower mass flow rate. This is because the effective height between the heater and cooler is less, which is responsible for generating buoyancy force shown in Fig.5.18. As a consequence, the buoyancy force is reduced, which leads to a reduction in mass flow rate.

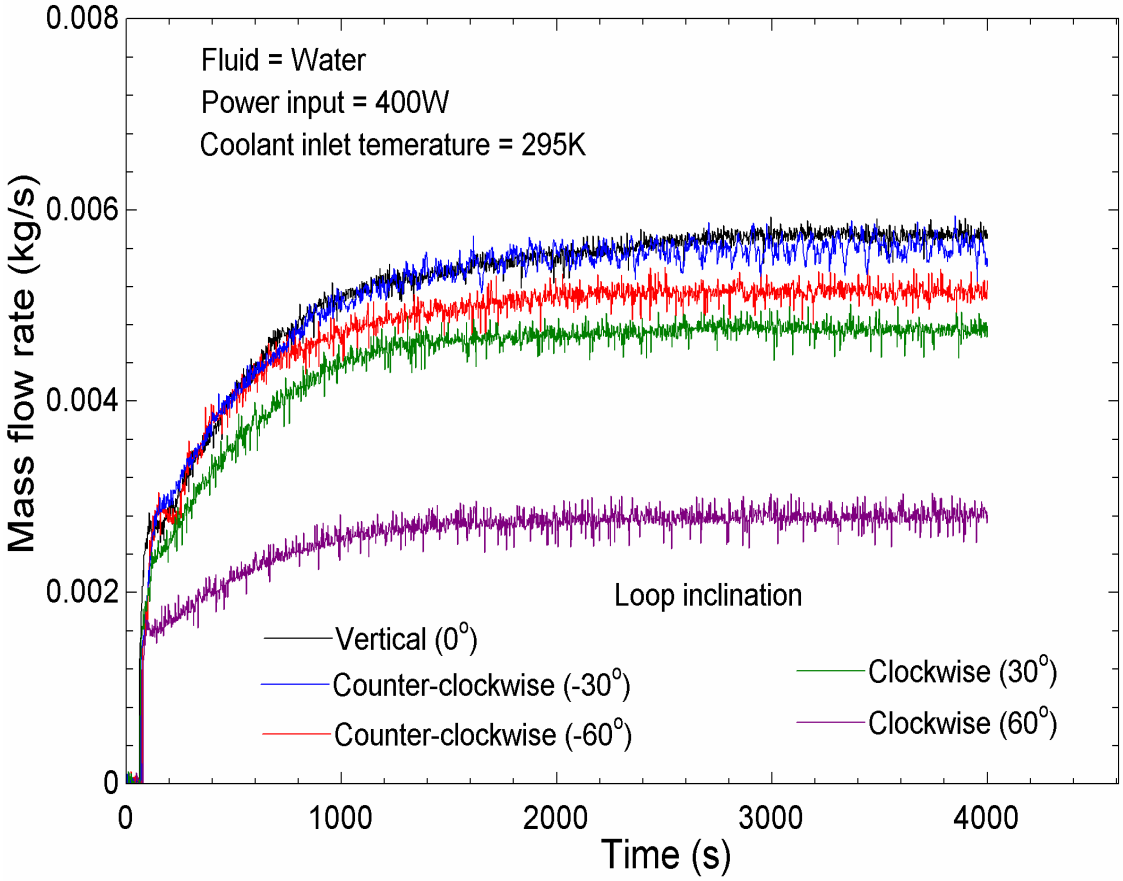

Fig. 5.17 Experimental transient mass flow rate for different loop inclinations

Figure. 5.19 show the steady state mass flow rate at different loop inclination for water and water-based mono/hybrid nanofluids at 400 W. It can be seen that increasing loop inclination on either side reduces the mass flow rate for all the working fluids. The reduction in mass flow rate is observed at about 2% and 9% for Counter-clockwise loop inclination and 17% and 49% for Clockwise loop inclination at 30^0 and 60^0, respectively, as compared to vertical loop (0^0) for water.

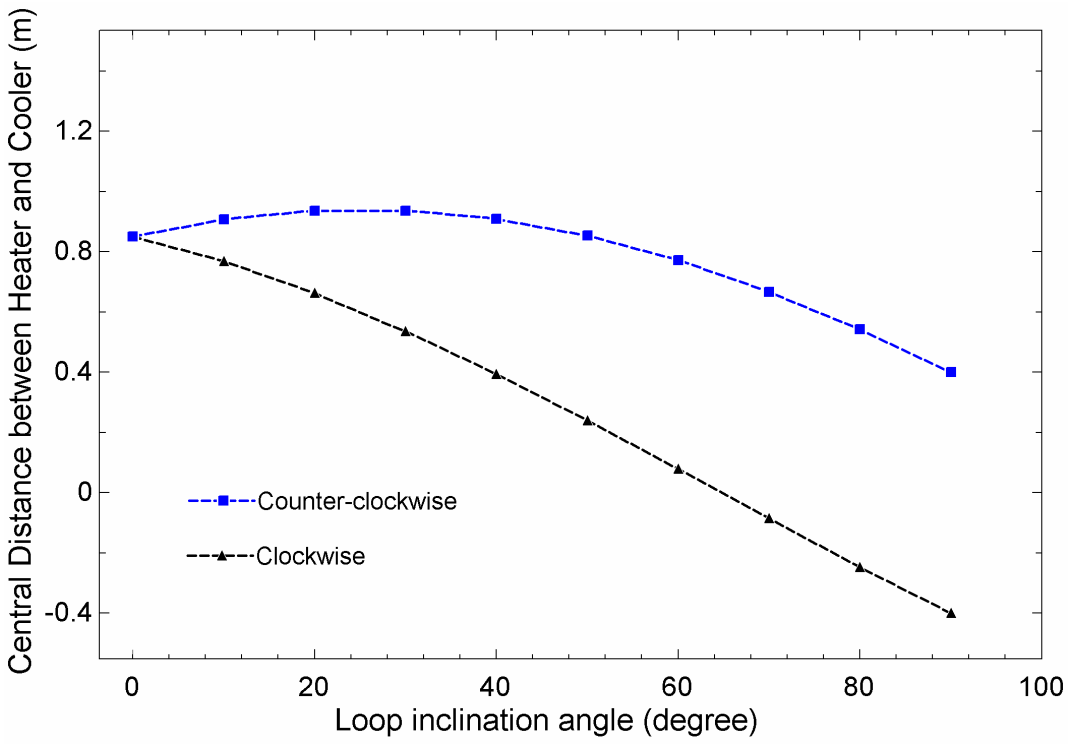

Fig. 5.18 Variation of the central distance between heater and cooler at different loop inclination

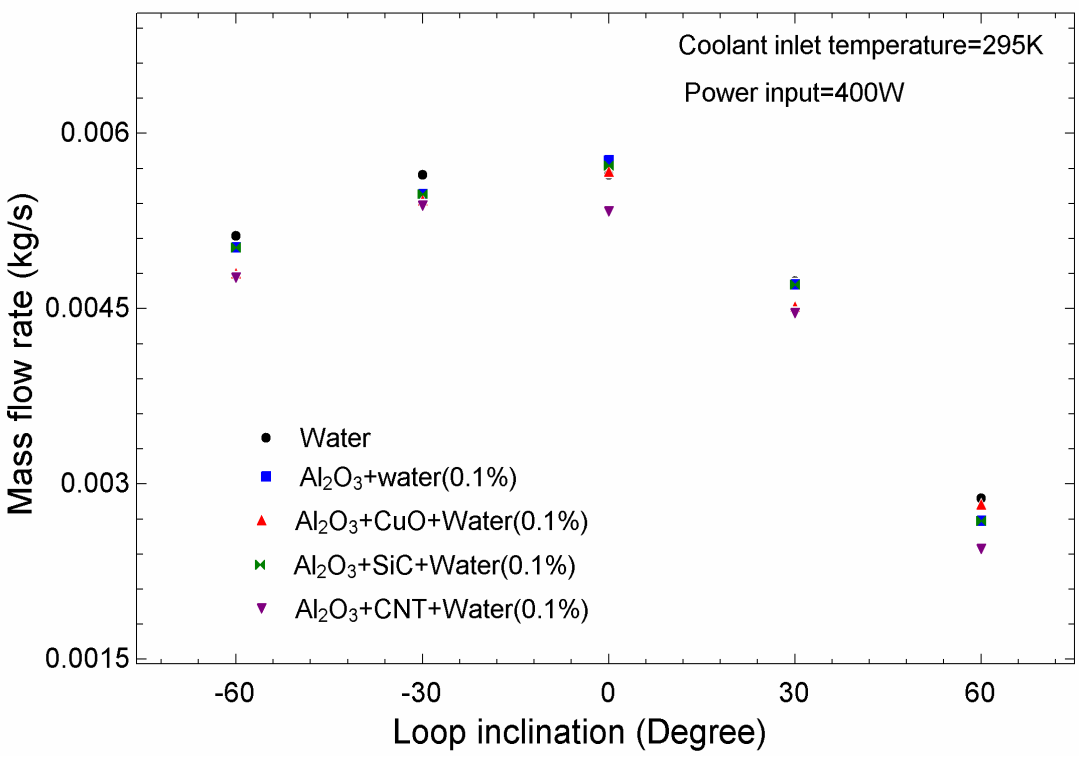

Fig. 5.19 Steady state experimental mass flow rate for different water-based mono/hybrid nanofluids at different loop inclinations

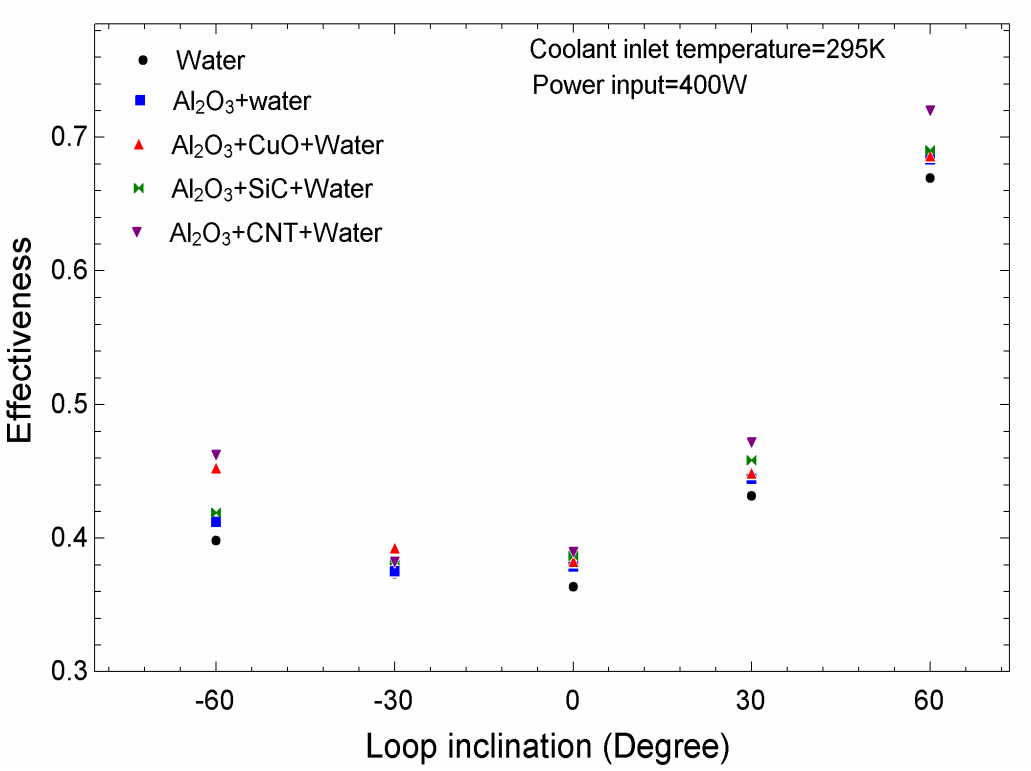

Fig. 5.20 Steady state experimental effectiveness for different water-based mono/hybrid nanofluids at different loop inclinations

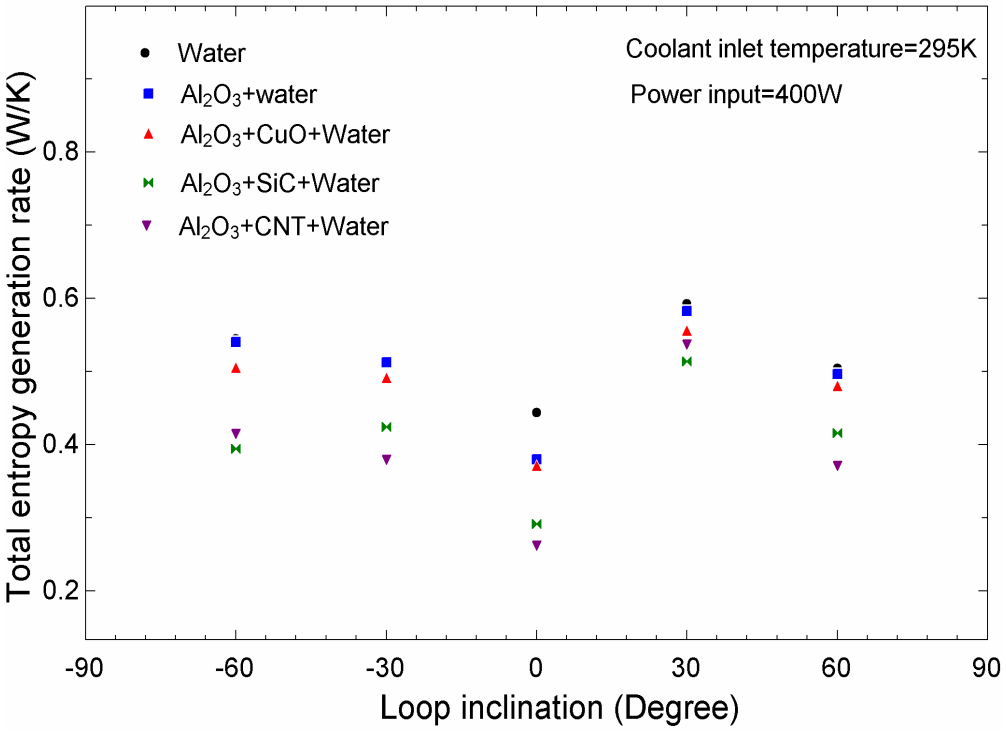

Fig. 5.21 Steady state experimental effectiveness for different water-based mono/hybrid nanofluids at different loop inclinations

Figure.5.20 reveals that the effectiveness of the heat exchanger increases with the loop inclination. This is attributed to the decreasing mass flow rate with the increasing loop inclination. This leads to an increase in the temperature difference ($T_{C,in}$-T_{Cout}). The heat transfer coefficient decreases due to a decrease in mass flow rate, which increases the heat exchanger outlet temperature; hence the temperature difference ($T_{C,in}$-$T_{S,in}$) increases. Since both temperature differences ($T_{c,in}$-$T_{c,out}$) and ($T_{C,in}$-$T_{S,in}$) increase, the overall effect will depend on which has a higher rate of increment. The rate of increment in the numerator is higher than the denominator; hence the effectiveness is increased. The increase in effectiveness is observed at about 3% and 10% for Counter-clockwise loop inclination and 18% and 84% for Clockwise loop inclination at 30^0 and 60^0, respectively, as compared to vertical loop (0^0) for water.

The effect of loop inclination on the entropy generation for water and water based mono/hybrid nanofluids is shown in Fig. 5.21. It is observed that the total entropy generation increases with the increasing loop inclination on both sides compared to the vertical loop for all the working fluids. The increase in entropy generation is observed at about 15% and 22% for Counter-clockwise loop inclination and 33% and 13% for Clockwise loop inclination at 30^0 and 60^0, respectively, as compared to vertical loop (0^0) for water.

5.4 Important findings

- Early flow initiation and higher mass flow rate are observed in spherical-shaped nanoparticle-based hybrid nanofluids compared to cylindrical-shaped nanoparticle-based hybrid nanofluids and water.

- The steady-state mass flow rate and total entropy generation increase, and effectiveness decreases with increasing power input for all fluids.
- The Al_2O_3+MWCNT+Water hybrid nanofluid shows batter performance since it has higher effectiveness and the lowest total entropy generation rate compared to other studied hybrid nanofluids and water.
- Increasing coolant inlet temperature increases the mass flow rate and total entropy generation rate and decreases the effectiveness for all fluids.
- The loop inclination decreases the mass flow rate, whereas it increases the effectiveness and total entropy generation rate. The Counter-clockwise inclination of the loop shows a lower reduction in mass flow rate compared to the clockwise inclination due to less reduction in the central distance between heater and cooler.